



HAL
open science

Stability and catalytic properties of 1T-MoS₂ obtained via solvothermal synthesis

Santiago Palencia-Ruiz, Denis Uzio, Chistèle Legens, D. Laurenti, P. Afanasiev

► **To cite this version:**

Santiago Palencia-Ruiz, Denis Uzio, Chistèle Legens, D. Laurenti, P. Afanasiev. Stability and catalytic properties of 1T-MoS₂ obtained via solvothermal synthesis. *Applied Catalysis A : General*, 2021, 626, pp.118355. 10.1016/j.apcata.2021.118355 . hal-03373385

HAL Id: hal-03373385

<https://hal.science/hal-03373385>

Submitted on 2 Nov 2021

HAL is a multi-disciplinary open access archive for the deposit and dissemination of scientific research documents, whether they are published or not. The documents may come from teaching and research institutions in France or abroad, or from public or private research centers.

L'archive ouverte pluridisciplinaire **HAL**, est destinée au dépôt et à la diffusion de documents scientifiques de niveau recherche, publiés ou non, émanant des établissements d'enseignement et de recherche français ou étrangers, des laboratoires publics ou privés.

Stability and catalytic properties of 1T-MoS₂ obtained via solvothermal synthesis

Santiago Palencia-Ruiz^{a,b}, Denis Uzio^b, Christèle Legens^b, Pavel Afanasiev*^a, Dorothée Laurenti*^a

^a Univ Lyon, Univ. Claude Bernard Lyon 1, CNRS, UMR5256, IRCELYON, F-69626, Villeurbanne, France.

^b IFP Energies Nouvelles, Rond-point de l'échangeur de Solaize, BP 3, F-69360 Solaize, France.

Abstract

Nanodispersed MoS₂ and CoMoS₂ materials containing metastable 1T MoS₂ phase have been prepared by solvothermal technique, characterized with several physico-chemical methods and evaluated in the electrocatalytic hydrogen evolution (HER), thiophene hydrodesulfurization (HDS) and 1-pentene hydrogenation (HYD) reactions. The role of different factors in the stabilization of 1T MoS₂ phase has been studied. Stability of 1T polymorph upon heating was followed by XPS and Raman spectroscopies and evolution of HER activity. The results of characterizations (Raman, XPS, TEM, XRD) converge to the conclusion that ethylene glycol intercalated between the MoS₂ layers stabilizes 1T –MoS₂ polymorph. When heated above 200 °C, the solids lose the intercalated ethylene glycol molecules and are transformed to 2H –MoS₂. The presence of cobalt does not influence the stability of 1T phase, but improves both HER and HDS performance due to formation of CoMoS species.

Keywords: molybdenum sulfide; hydrogenation; thiophene hydrodesulfurization; hydrogen evolution electrocatalyst

1. Introduction

Molybdenum disulfide (MoS₂) is a material important in the fields of lubrication, catalysis, sensing, energy storage or electronics [1,2,3, 4]. MoS₂ is widely applied as active phase in hydrotreating catalysis, aiming at the reduction of sulfur contents in fuels via hydrodesulphurization reaction (HDS), in which organosulfur molecules react with hydrogen [5,6,7]. Recently MoS₂ received much attention as a prospective material for modern technologies such as batteries [8], supercapacitors [9], hydrogen storage [10], photocatalysis [11,12] and in particular as a cathode material for hydrogen evolution reaction (HER), aiming to replace noble metals [13,14,15].

MoS₂ is a layered compound that can exist under several polymorphic phases, 1T, 2H and 3R. The

thermodynamically stable 2H-MoS₂ phase exist in nature as molybdenite mineral. In 2H-MoS₂, Mo atoms are coordinated by sulfur in a trigonal-prismatic geometry, forming covalent 2D slabs. The slabs interact only via Van der Waals forces. The metallic 1T phase with octahedral coordination of Mo atoms is metastable [16, 17] and shows higher electrocatalytic and photocatalytic HER activity because of easier charge transfer as compared with semiconductor 2H-MoS₂ [18, 19, 20].

Conventional HDS catalysts contain nanodispersed 2H-MoS₂ phase. In the MoS₂ nanoparticles, catalytic sites are located at the edges of slabs, for both non-promoted and Co- or Ni- promoted catalysts [21]. Therefore, the catalytic HDS activity (or electrocatalytic HER activity) of 2H-MoS₂ is proportional to the amount of the exposed edges [22]. For the 1T-MoS₂ it was argued that its basal planes are active, though the mechanisms are vividly debated [23, 24]. Higher electrochemical activity of the 1T phase makes it more attractive as HER cathode than the 2H counterpart. However, metastability of the 1T-MoS₂ is a serious obstacle, which limits its applications. Few examples of 1T phase application in heterogeneous catalysis were reported, mostly for methanethiol synthesis from syngas [25, 26], perhaps because of insufficient thermal stability. Recent literature reports on the stabilization of 1T phase in hydrothermal [27, 28] or solvothermal preparations using organic solvents [29]. Stabilization of 1T-phase was observed for both Co- doped and sole Mo solvothermal preparations using ethylene glycol (EG) solvent [30, 31]. The reason of 1T phase stabilization in these preparations and the role of cobalt are not clear. Earlier, we carried out similar preparations using EG as a solvent and elemental sulfur as a sulfiding agent, but we did not observe formation of the 1T phase [32, 33].

In this work we explore the properties of the 1T-MoS₂ solvothermal preparations with and without cobalt addition and compare them with the benchmark references in the HER and HDS test reactions. The goal is to give an insight into the stability of 1T phase in these preparations and its role in HER electrocatalysis and HDS or hydrogenation (HYD) heterogeneous catalysis.

2. Experimental

2.1. Materials preparation

All reactants were high purity grade purchased from Aldrich. The preparation used solvothermal process in EG as described in [22]. Cobalt acetate tetrahydrate, sodium molybdate dihydrate and elemental sulfur were used as precursors with S:Mo atomic ratio of 2 and (for cobalt-containing solid) Co:Mo ratio of 0.4. The corresponding solvothermal samples are designated respectively as Sol_NaMoS₂ and Sol_Co_NaMoS₂. Reference CoMoS solid containing only 2H-MoS₂ and designated as PPC_CoMoS was prepared by means of ambient pressure reflux of elemental sulfur, ammonium heptamolybdate and

cobalt nitrate in propylene carbonate (PPC), as described elsewhere [34]. Reference 2H-MoS₂ was prepared from the decomposition of ammonium thiomolybdate (ATM) at 450°C as described in [25] and designated as 2H_ATM_MoS₂. Potassium - stabilized reference 1T phase designated as K_H₂O_MoS₂ was prepared by sulfidation-reduction of potassium molybdate, followed by partial oxidation in presence of water, as described by Wypych et al [10].

2.2 Characterizations.

The X-ray photoelectron spectroscopy (XPS) experiments were carried out on a KRATOS AXIS Ultra DLD spectrometer. The samples were prepared in a glove box under argon atmosphere, by pressing the powders onto an indium foil. The spectra were acquired using monochromatic Al K α radiation (1486.6 eV, 150 W), and the binding energies (BE) were corrected taking C 1s (284.6 eV) as the reference. Decomposition of the S 2p and Mo 3d XPS signals was carried out using the oxide and sulfide references. The effective atomic concentrations were obtained from the areas of the corresponding peaks corrected with respect to the sensitivity factors.

Nitrogen adsorption isotherms were measured on a Micromeritics ASAP 2010 instrument. Specific surface area and pore size distribution were determined using BET and BJH equations, respectively. Prior to measurements, the samples were outgassed in vacuum at 200 °C for 2h. The X-ray diffraction (XRD) patterns were obtained on a Bruker diffractometer with Cu-K α emission and crystalline phases were identified using standard JCPDS files. Mean size of coherent scattering domains was determined using the Scherrer equation, and Rietveld refinement algorithm. For the XRD study at high temperature, the diffractometer used was a PANalytical X'Pert Pro. Patterns were acquired from RT to 600°C every 50°C with a temperature ramp of 5°C/min. In order to be close to the reaction operating conditions, hydrogen flow of 1 L/h passed through the sample. Transmission electron microscopy (TEM) was carried out on a JEOL 2010 device with an accelerating voltage 200 keV. The samples were dispersed in ethanol by ultrasound and then put onto a lacey carbon on a copper grid. The analysis of images was carried out using Gatan Digital Micrograph™ software. The Co and Mo content in the solids was determined, after dissolution in a HNO₃/H₂SO₄ mixture, by plasma-coupled atomic emission spectroscopy (ICP-ES Activa Jobin Yvon). Elemental analysis of light elements (CHNS) was performed on an analyzer Thermo Fisher Flash 2000. Raman spectra were recorded with a LabRam HR Raman spectrometer (Horiba-Jobin Yvon) equipped with BXFM confocal microscope, interference and Notch filters and charge-coupled device detector. The exciting line of a laser (Melles Griot) at 514 nm was focused using a x 50 long working distance objective with a maximum of 0.1 mW for the laser power. The spectra collected with gratings

of 1800 grooves.mm⁻¹ were accurate within 1 cm⁻¹.

Thermal analysis was carried out under nitrogen flow. TGA-DSC METTLER thermobalance coupled to a quadrupolar mass spectrometer (Thermostar/Pfeiffer) was used. Samples were heated from RT to 600°C with temperature ramp of 5°C/min under a nitrogen gas flow (25 ml/min).

2.3. Electrochemical measurements.

To prepare the catalytic inks, 10 mg of a sulfide material powder was ultrasonically dispersed in a mixture containing 800 µl of ethanol and 400 µl of 0.5% Nafion solution, containing 2 mg of carbon (acetylene black). To prepare working electrode, 10 µl of catalytic ink suspension was dropped onto rotating glassy carbon electrode (0.196 cm²) and dried. The catalyst loading was 0.6 mg/cm². The electrochemical measurements were performed on a Voltalab three-electrode potentiostat using a Pt counter electrode and SCE reference electrode at 25 °C in purged solutions of 0.5 M H₂SO₄, by bubbling argon. CV plots for determining ECSA were obtained in the non-faradaic potential range from -0.1 to 0.1 V vs. SCE at scan rates ranging from 10 to 300 mV/s. Linear Sweep Voltammetry (LSV) scans were carried out at 5 mV/s rate.

2.4. Thiophene HDS and 1-pentene HYD

Catalytic activities in thiophene hydrodesulfurization (HDS) and pentene hydrogenation (HYD) reactions were measured at atmospheric pressure in a fixed-bed flow microreactor. The same experimental set-up was used for both reactions, by replacing liquid thiophene with 1-pentene in the saturator with appropriate temperature to deliver the target partial pressure for each.

HDS reaction was carried out in the temperature range 240–320°C, under 15 ml/min gas flow, using 100–200 mg of catalyst and partial pressure of thiophene of 2.7 kPa. The plug-flow reactor model was used to calculate the specific reaction rate, V_s , according to the equation (1):

$$(1) \quad V_s = - (F/m) \ln(1 - x)$$

where x is the total thiophene conversion, F is thiophene molar flow (mol/s), m is the sulfided Mo mass in the catalyst deduced from XPS and ICP-OES information (g). The catalytic activities were compared at steady state conversion, after 16 h on-stream with the initial temperature. Arrhenius plots using four temperature points between 280 and 340 °C were built to attest kinetic regime and to estimate activation

energy. Correlation coefficient better than 0.99 and physically meaningful activation energy between 17 and 22 Kcal/mol mean successful activity measurement. HYD reaction of 1-pentene was carried out under the same flow conditions as thiophene HDS in the temperature range 160–200 °C, under 15 ml/min gas flow, using 100–200 mg of catalyst and partial pressure of 1-pentene of 11 kPa and the catalytic rates were calculated using the same pseudo-first order reaction.

3. Results and discussion

3.1. Characterizations aimed at identification of 1T-MoS₂ phase.

XRD patterns of two solvothermal solids, compared with the 2H_ATM_MoS₂ reference, are shown in Fig .1. For both samples, the (002) peak attests increased interlayer distance (ID) of \approx 1.08 nm and \approx 1.02 nm for Sol_Co_NaMoS₂ and Sol_NaMoS₂ respectively, as compared to 0.62 nm for reference ATM. The increased ID could be attributed to intercalation of sodium and/or cobalt ions as well as organic molecules between the layers. Previously, intercalation of sodium into MoS₂ led to the ID not exceeding 0.72 nm [35]. Higher ID have been observed for organic molecules intercalated between the MoS₂ [36, 37, 38]. In our case, ethylene glycol molecules might be intercalated. Noteworthy, in our previous studies using EG as a solvent for MoS₂ preparations, no increase of ID has been observed [24, 25], probably because both the Mo source and reaction time were different. For Sol_Co_NaMoS₂, no crystalline cobalt compounds were detected in the XRD patterns, in agreement with work by Li et al. [22].

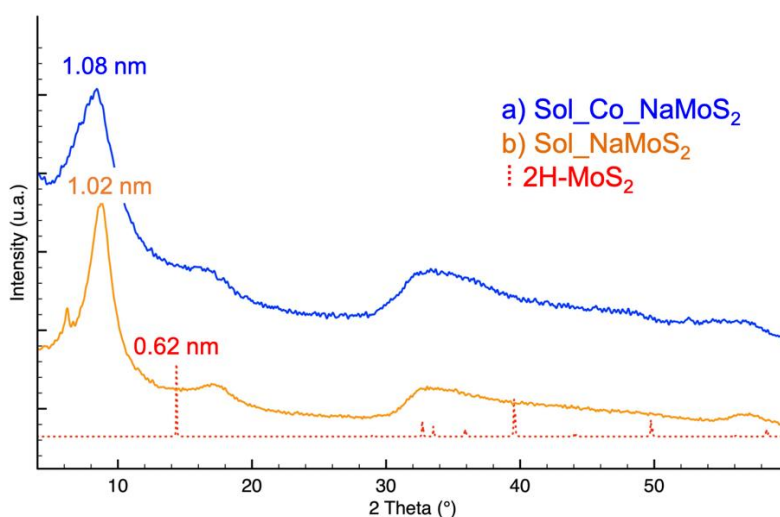


Figure 1. Room temperature XRD patterns of freshly prepared (a) Sol_Co_NaMoS₂ (b) Sol_NaMoS₂ and 2H-polytype library pattern PDF-00-037-1492

The elemental analysis results are displayed in Table S1 (Suppl. Mat.). Freshly prepared solids have the respective empirical formulae $C_{1.2}H_{3.4}O_{1.5}Na_{0.2}MoS_{1.5}$ and $C_{1.5}H_{3.9}O_{2.1}Co_{0.5}Na_{0.2}MoS_{1.8}$. Both solids are sulfur-deficient with respect to the composition corresponding to a complete sulfidation towards the MoS_2 and CoS_2 sulfides. This lack of sulfur could arguably be beneficial for the formation of 1T-polytype as suggested previously [39, 40].

Despite intense washing, considerable amount of sodium remained in both materials, at the atomic Na:Mo ratio of 0.2. We suggest that this residual sodium, hard to remove by washing, is intercalated between the MoS_2 layers. The amount of sodium in both materials is close to the minimal value needed to stabilize the 1T polytype, as reported [41]. Besides, the stoichiometry of CH and O for both materials approximately corresponds to that of ethylene glycol molecule. It seems that interlayer distance (ID) is increased due to the presence of both sodium cations and organic molecules between the MoS_2 layers. Note that the increased ID per se does not equate to stabilization of the 1T phase but merely correlates with it in some cases.

TEM images of Sol_NaMoS₂ and Sol_Co_NaMoS₂ solids are shown in Fig. 2 and Fig S1. For the Sol_NaMoS₂ solid, spherical agglomerates are observed at low magnifications (Fig.2a). Cobalt-containing solid is composed by 100-300 nm size agglomerates with a hollow-spherical morphology (Fig 2e). The agglomerates for both solids consist of weakly oriented bundles of slabs of 10-20 nm length. At high resolutions, frontal projection images attest that the slabs are highly defected and zigzag Mo atoms structures typical for 1T phase are present (Fig. 2d) (Note that the theory resolution of HRTEM JEOL 2010 is 0.19 nm, sufficient to resolve the atomic structure at stake. In practice conventional HRTEM is usually inappropriate to observe 2D structure of MoS_2 nanoscopic slabs, STEM HAADF being by far preferable. However, for the samples containing extended and thin slabs as our samples, the 2D structure was successfully resolved). Similar morphology was observed with or without cobalt, but rare CoS_2 particles of about 10 nm were observed by dark-field HRTEM. This CoS_2 phase could not be observed by XRD probably because of its small amount. Remarkably, the increased ID of 1.08 or 1.03 nm, as calculated from XRD, was never observed in TEM images. The ID measured from TEM images was sometimes near the 0.72-0.73 nm value typical for Na-intercalated MoS_2 and sometimes it was close to 0.62 nm of the 2H phase (Fig. 2c, Fig S1b, d). Such difference between the ID measured by TEM and XRD could be attributed to the differences in the measurement conditions. Indeed, XRD was carried out at ambient conditions and at weak doses of X-ray irradiation, whereas TEM measurement requires high vacuum and high brilliance of the electron beam. If organic molecules are present between the layers

they could be partially eliminated by vacuum and/or radiation in TEM, whereas XRD method is non-invasive. The observed ID difference suggests that EG-intercalated MoS₂ structure collapsed under TEM conditions, towards partially Na-intercalated phase (because sodium remains between the layers even under vacuum).

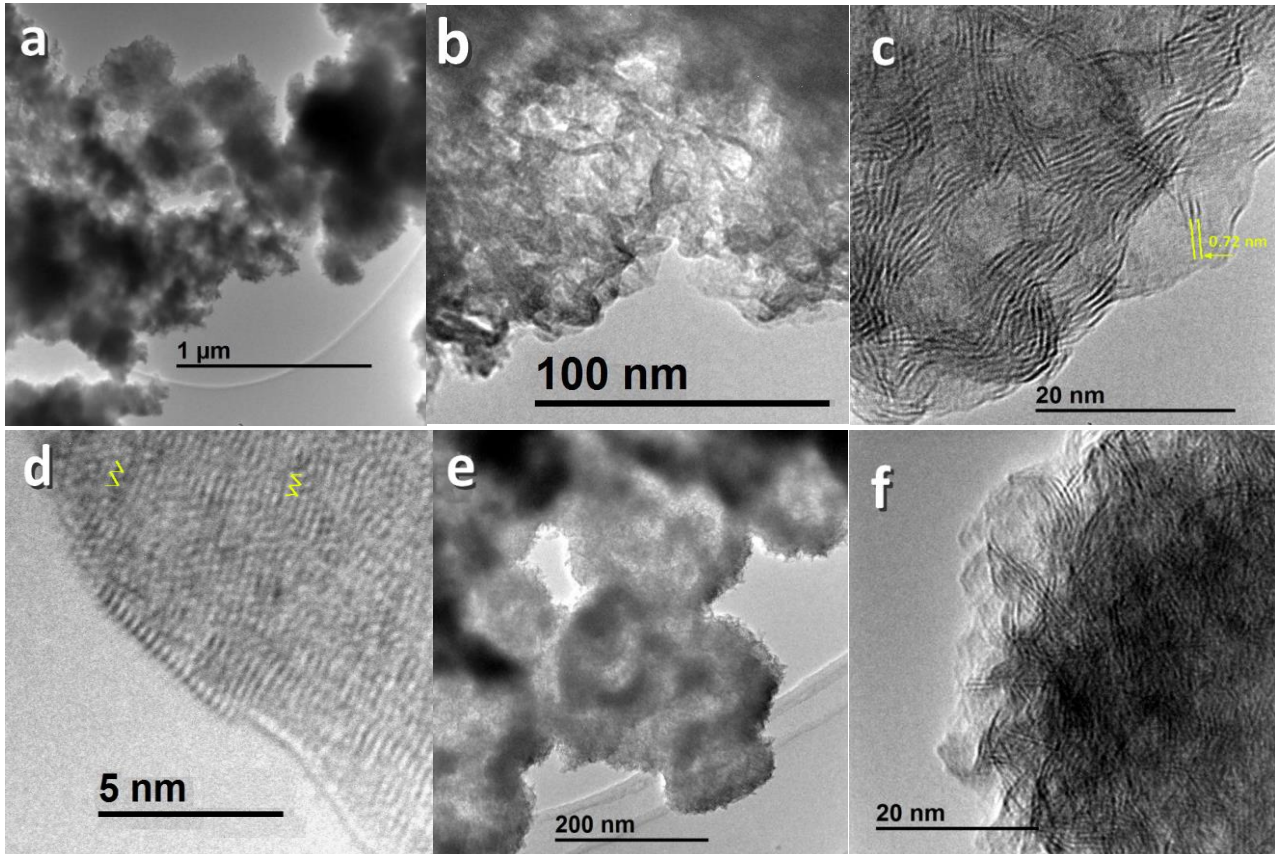


Figure 2. TEM images taken at different magnifications of the solids Sol_NaMoS₂ (a-d) and Sol_Co_NaMoS₂ (e,f).

Raman spectra of the materials under study are presented in Fig. 3 in comparison with the spectra of references: MoO₃, potassium-stabilized 1T phase sample 1T K_H₂O_MoS₂ and 2H - ATM_MoS₂. The spectra of both solvothermal materials do not display the signatures of MoS₂, because of fluorescence caused by high content of organics. Li *et al.* [22] claimed to observe typical signatures of 1T polytype for the products of similar preparation. However, when we increased the incident laser power from 100 μW to 1 mW, the solvothermal samples were oxidized and the peaks of MoO₃ appeared in the low-frequency part, matching approximately with the characteristic peaks J₁-J₃ of 1T phase (Fig. S2). Several MoO₃ peaks below 500 cm⁻¹ appearing due to oxidation by laser beam could be misinterpreted as 1T phase. However, a striking difference exists at higher wavelengths, in particular above 800 cm⁻¹, where

strong lines of Mo=O vibrations are observed. Therefore, for identifying 1T phase with Raman spectroscopy, this region should be checked.

Overall, XRD and TEM attest that two MoS₂ – based materials with increased ID have been obtained, intercalated by ethylene glycol and sodium. One of two solids contains cobalt, but there is no indication that cobalt is intercalated between the sulfide layers. High-resolution TEM suggests formation of 1T phase. However, the intercalated EG molecules hinder Raman identification of the MoS₂ signal, so we could not conclude whether 1T phase was predominant or not.

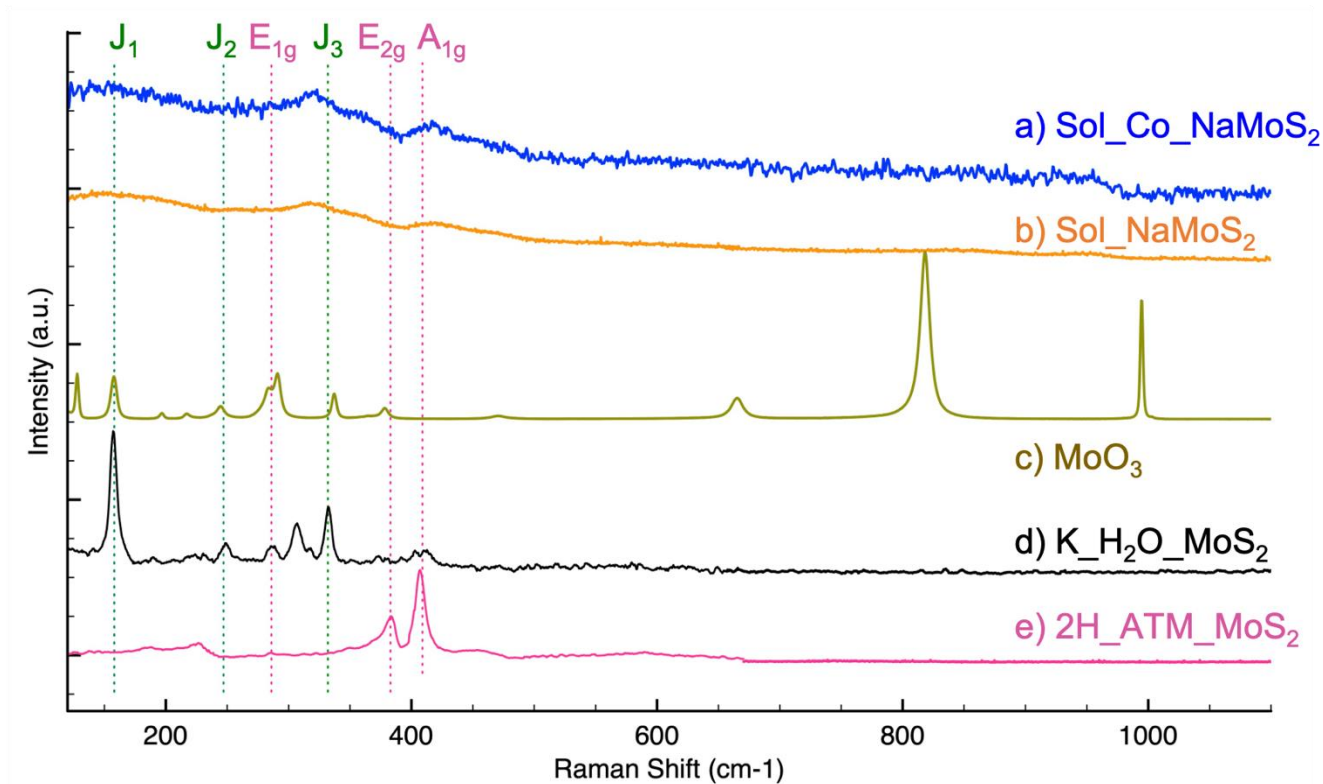


Figure 3. Room-temperature Raman spectra of (a) Sol_Co_NaMoS₂ and (b) Sol_NaMoS₂. For comparison, spectra of references are given: MoO₃ (c), 1T polytype K_H₂O_MoS₂ (d) and 2H_ATM_MoS₂ (e). E and A modes of 2H phase are indicated by pink dotted lines and J modes of 1T phase - by green dotted lines.

To resolve this uncertainty XPS characterization has been carried out for both materials in the Mo 3d, S 2p and Co 2p regions (Fig. 4 and Fig. S3). Table 1 summarizes the binding energies (BE) and the percentage of the elements obtained from analysis of Mo 3d and S 2p spectra. For both solids, the decomposition of Mo 3d signal reveals a peak with BE by 0.9 eV lower than the Mo(IV) peak in 2H-MoS₂, but fitting with the K_H₂O_MoS₂ reference and with the literature XPS spectra for MoS₂ 1T polytype [42, 43]. Simultaneously, a shift toward lower BE was observed in the S 2p region, corresponding to sulfur signal in the 1T-MoS₂. For both catalysts, the XPS contribution of the 1T phase was much higher than that of 2H MoS₂. Both solids contain also considerable amounts of Mo(V) and

Mo(VI) oxide species. The S 2p doublet located between 163 and 165 eV was assigned to S_2^{2-} in Mo oxysulfide species ($Mo-O_xS_y$), confirming the presence of Mo(V). For the Co-containing solid, two peaks were also observed at 168.7 and 169.9 eV corresponding to sulfate species which indicate that surface sulfur atoms were also partially oxidized due to short air exposure. The presence of Mo oxide species in XPS agrees with the ratio $S/Mo < 2$ as found by elemental analysis. However, the XPS $S(1T)/Mo(1T)$ and $S(2H)/Mo(2H)$ ratios for Sol_NaMoS₂ solid are respectively 2.8 and 2.2.

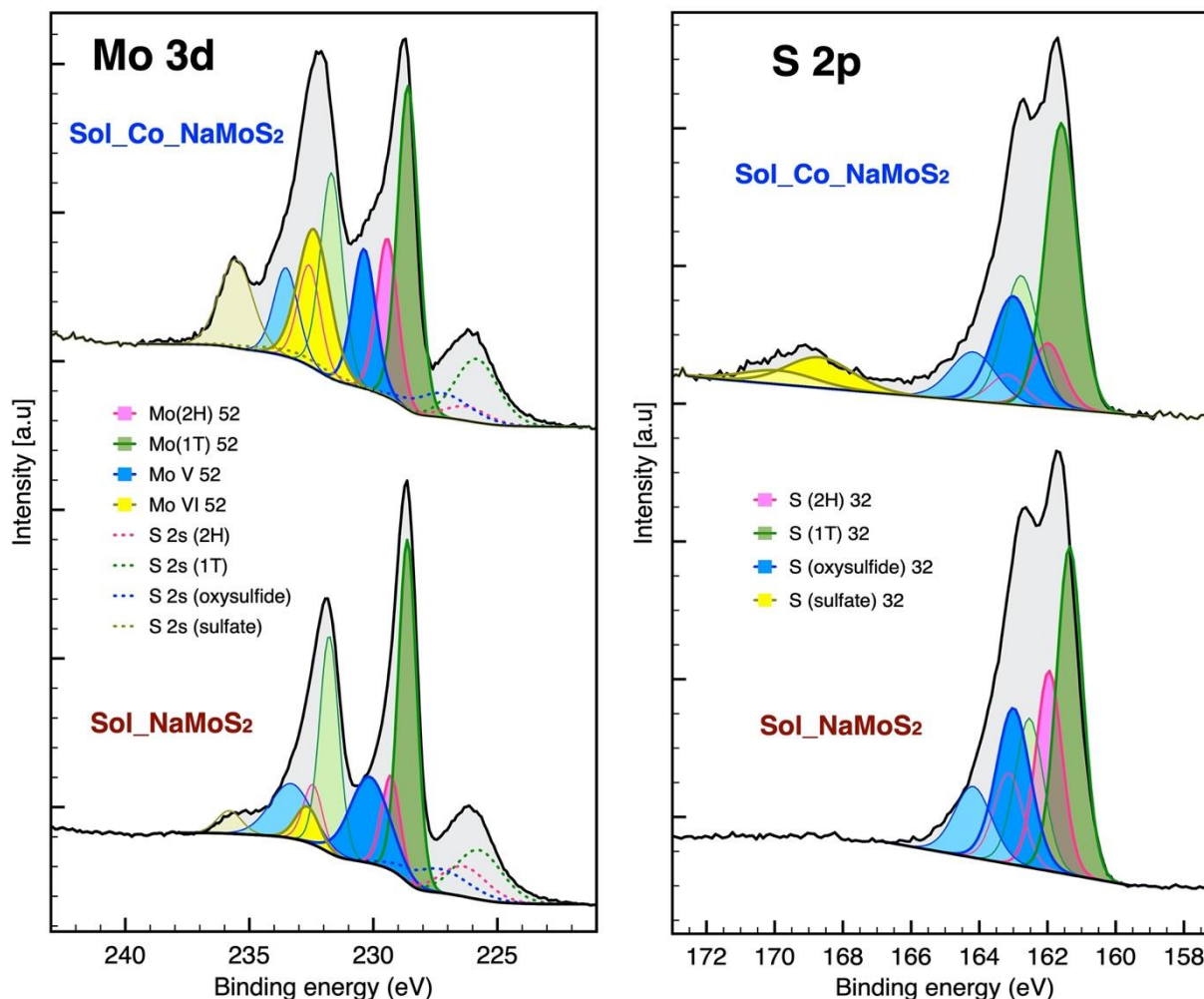


Figure 4. X-ray photoelectron spectroscopy of Mo 3d and S 2p regions Sol_Co_NaMoS₂ and Sol_NaMoS₂ obtained from decomposition.

For the Co-containing material, the Co 2p signal (Table 1, Figure S3) contains major contribution from Co(II) oxide (~65%), a slight contribution of Co sulfide (~5 %) and considerable amount of CoMoS promoted phase (~30 %). Overall, XPS attests the presence of the 1T polytype in the solvothermal preparations under study. In both solids, 1T surface contribution represents around 30% at. of the total

Mo and 65-70% of total sulfide phase.

Table 1. XPS Binding energies (BE) from the Mo 3d and S 2p decomposition and concentration in at. % XPS Decomposition of Mo 3d. S 2p Binding Energy (BE), relative atom amount (%) of Mo, S in Sol_NaMoS₂ and Sol_Co_NaMoS₂ before and after heating at 350°C under H₂.

	Catalyst	Mo3d _{5/2} (2H)	Mo3d _{5/2} (1T)	Mo3d _{5/2} V	Mo3d _{5/2} VI	S2p _{3/2} (2H)	S2p _{3/2} (1T)	S2p _{3/2} (oxysulfide)	S2p _{3/2} (sulfates)
BE (eV)	Sol_NaMoS ₂ (RT)	229.3	228.6	230.2	232.7	162.0	161.4	163.0	-
%		14.1	51.0	28.0	6.9	27.4	44.9	27.8	-
BE (eV)	Sol_NaMoS ₂ 350°C H ₂	229.0	228.3	230.0	232.4	161.8	161.2	163.0	168.1
%		82.5	0.1	7.4	10.0	81.1	0.1	12.2	6.6
BE (eV)	Sol_Co_NaMoS ₂ (RT)	229.4	228.6	230.4	232.4	162.0	161.6	163.0	168.7
%		18.8	38.3	18.1	24.8	11.6	51.6	25.4	11.5
BE (eV)	Sol_Co_NaMoS ₂ _350°C H ₂	229.1	228.5	230.0	232.4	161.9	161.5	163.3	168.3
%		58.3	0.6	13.0	28.2	71.9	1.1	14.1	13.0

Hydrogen evolution reaction (HER) was applied here as a characterization method rather than a target application. Indeed, the differences of HER performance between 1T and 2H phases are well-known to be very strong and therefore should be indicative to distinguish between two polytypes. LSV curves and the corresponding Tafel plots are shown in Fig. 5 and Fig. S4. High HER performance was observed for both solvothermal materials. Tafel slopes and overpotentials for the solids agree with the literature [44, 45] and are considerably lower than for the benchmark reference 1T phase K_H₂O_MoS₂ (Table 2). Low overpotentials as observed might be attributed to the combination of metallic character and high BET specific surface area (S_{BET}), near 100 m²/g. The HER mechanism seems to be limited by hydrogen desorption as the low values of Tafel slope suggest.

Notably, the electrochemical surface areas (ECSA) for both solvothermal products and for the K_H₂O_MoS₂ reference exceed their BET surface areas. By contrast, for 2H-MoS₂ and PPC_CoMoS references, BET surface area is considerably greater than ECSA (Table 2). These electrochemical responses could be ascribed to their different intrinsic conductivity. In agreement with the last observation, charge-transfer resistance (R_{CT}) of both solvothermal solids under study is close to that of

the K₂H₂O₂MoS₂ reference, evidencing their metallic character (independently of the presence of cobalt).

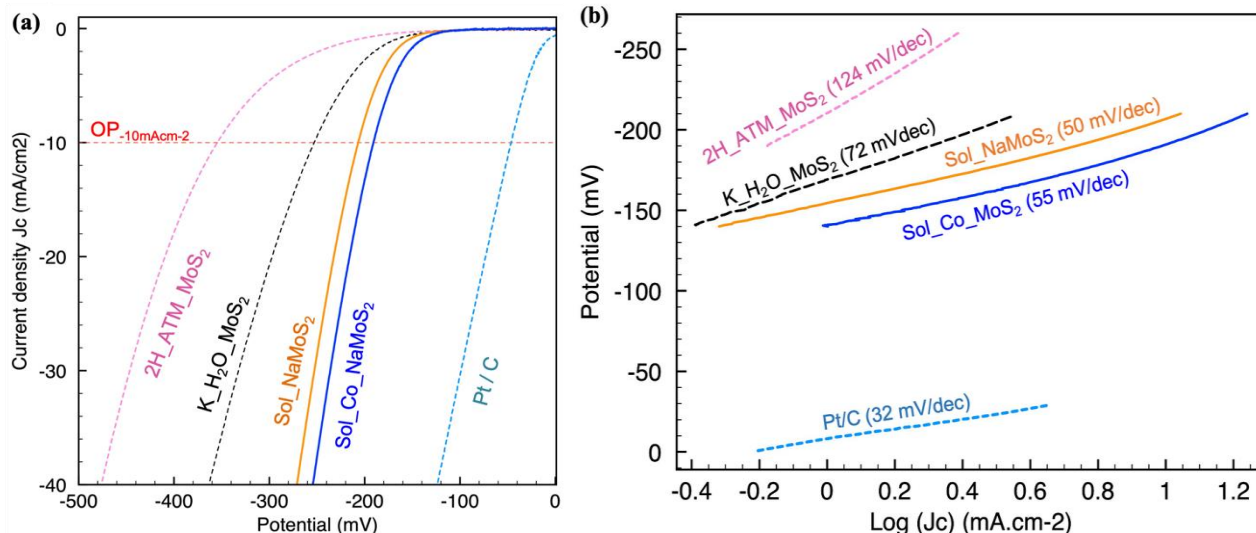


Figure 5. LSV curves obtained in 0.5 M H₂SO₄ at 5 mV/s rate (a) and Tafel plots (b) for solvothermal materials in HER reaction, in comparison with benchmark references.

The HER catalytic performance of Sol_{Co}NaMoS₂ and Sol_{Na}MoS₂, is quite similar, suggesting that contribution of cobalt is not as important as the nature of the polytype. HER results support the conclusion that 1T phase is obtained for both Co-doped and sole Mo materials. Our next goal was to clarify whether the 1T phase as prepared may be interesting for heterogeneous catalysis. Therefore, thermal stability under hydrogen has been studied, as follows.

Table 2. HER parameters and specific surface areas for the solids under study and benchmark references

HER	Sol _{Na} MoS ₂	Sol _{Co} NaMoS ₂	K ₂ H ₂ O ₂ MoS ₂	2H ₂ ATM ₂ MoS ₂	PPC _{Co} MoS	Pt / C
OP _{-10mA.cm-2} [mV]	-207	-191	- 253	- 355	-290	- 49
Tafel slope [mV/dec]	50	55	71	124	77	36
ECSA [m ² /g]	198	211	33	17	12	-
S _{BET} [m ² /g]	90	101	17	49	130	-
R _{CT} [Ω]	14	17	16	975	1146	-

3.2. Thermal stability of 1T-MoS₂.

Ex-situ Raman study was carried out after heating of the samples under hydrogen at different temperatures, from ambient to 350°C (Fig S5). For both catalysts no clear Raman modes were observed

below 200°C because of intercalated EG. At 200°C, the A_{1g} vibration mode of 2H-MoS₂ emerges. Notably this temperature matches with the boiling point of ethylene glycol (196°C). These Raman signals increase after heating at 250°C and finally at 350°C both solids present typical 2H-MoS₂ spectra (E_{2g} and A_{1g} , Fig S5). Therefore, Raman gives 200°C as a lower limit temperature after which 2H phase certainly began to crystallize.

XRD patterns of the solids heated under hydrogen are shown in Fig. S6 and S7. The ID of 1.03 nm ($2\theta = 8.8^\circ$) corresponding to $|001|_{1T}$ plane, shifted toward lower values after heating from 200°C onward, indicating deintercalation of EG. The ID gets close to that of 2H-MoS₂ (≈ 0.65 nm), but did not attain 0.62 nm value, probably due to remaining intercalated Na. In the Co-containing solid, Co₉S₈ phase was observed beside 2H-MoS₂ after heating at 350 °C

XPS study was performed after heating at 350°C under H₂ for 1 h (Table 1 and Figure 6) and showed total disappearance of the 1T-polytype contributions in both Mo 3d and S 2p regions. At the same time 2H phase contribution increased. For Sol_Co_NaMoS₂ sample the Co 2p region displays an increase of the CoMoS phase signal, as well as that of cobalt sulfide (Figure S3).

Thermogravimetric analysis shows mass losses of about 20 and 25% after heating in nitrogen from RT to 600°C Sol_NaMoS₂ and Sol_Co_NaMoS₂ respectively (Fig. S8). This agrees with the mass loss expected after removal of all EG. For both samples, a mass loss of about 4% was observed between RT and 120°C which corresponds to physisorbed water. Then, from 200 to 350°C, 15 to 20% mass is lost, corresponding to EG removal.

HER test was performed for the solids pre-heated under hydrogen at various temperatures (Fig. 7, Table S2). Tafel slope was considered as an intrinsic descriptor of the metallic character, because its variation is striking upon the phase transition. For the 1T phase Tafel slope stays in the range 50-75 mV/decade, whereas for 2H-MoS₂ polytype is greater than 100 mV/dec, namely 124 mV/dec for the reference. For Sol_NaMoS₂, the Tafel slope progressively increased upon heating and reached the value typical for 2H-MoS₂ after heating at 350°C. However, when cobalt is present, Tafel slope do not decrease considerably after heating up to 350°C, in spite of total conversion to 2H-MoS₂ (as evidenced by Raman and XPS).

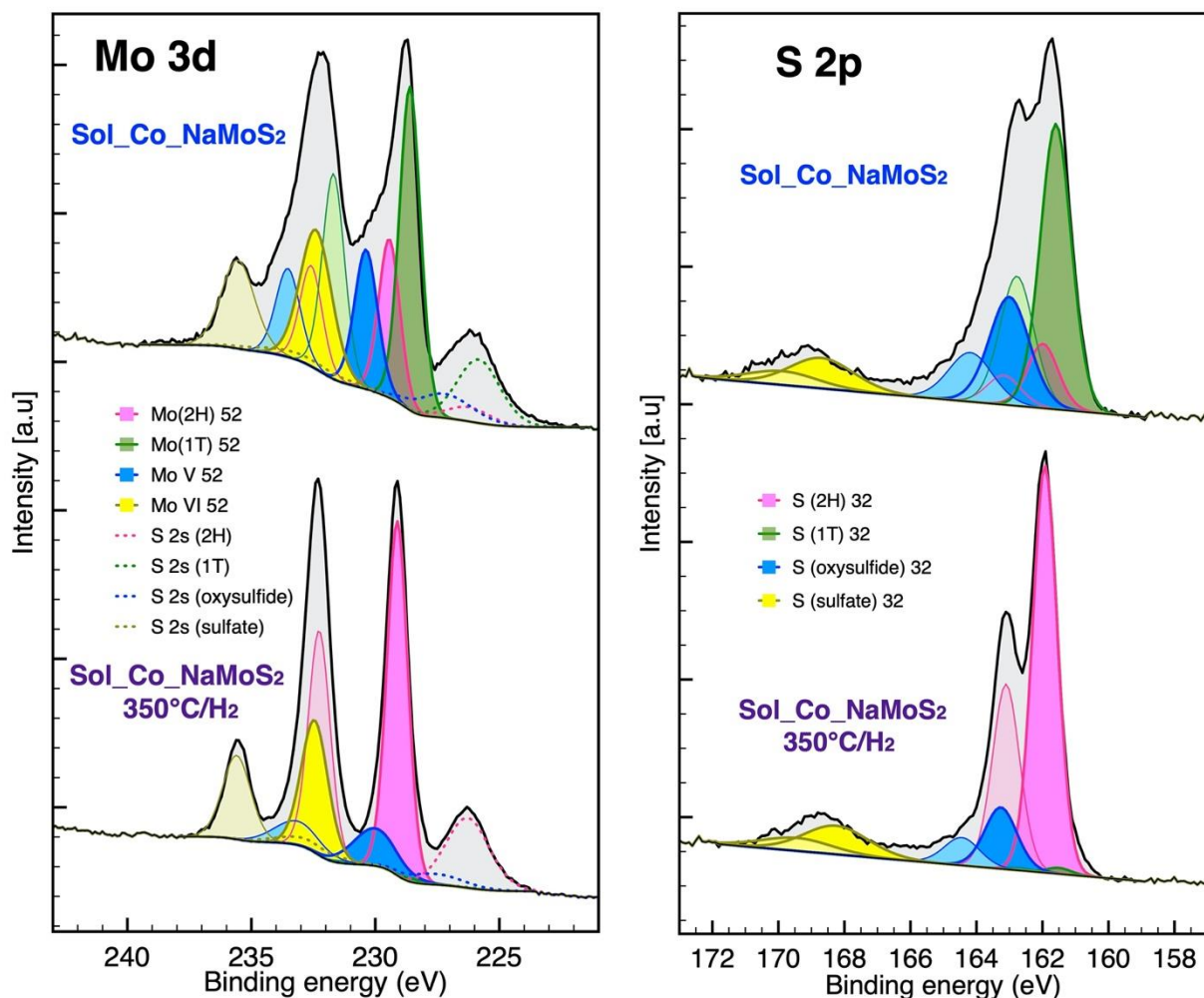


Figure 6. X-ray photoelectron spectroscopy of Mo 3d and S 2p regions of fresh (Sol_Co_NaMoS₂) and heated (Sol_Co_NaMoS₂_350°C) solid.

Therefore, cobalt improved the HER performance independently on the MoS₂ polymorph. To confirm this result, a CoMoS reference was tested for comparison that contains only 2H-MoS₂ (PPC_CoMoS). HER performance of the reference promoted catalyst revealed that cobalt strongly contributes to the Tafel slope and overpotential observed.

The ECSA values for freshly prepared samples are high whereas it drops for the heated sample and the CoMoS reference (Table. S2). Impedance spectroscopy shows the curves for which the equivalent circuit contains Warburg and charge transfer elements, the latter being diagnostic for the electric conductivity of our materials [46]. The charge transfer resistivity (R_{CT}) of reference 2H_ATM_MoS₂ and of Sol_NaMoS₂_350°C/H₂ is about an order of magnitude superior to that of Sol_NaMoS₂ (Figure S9, Table S2). These results confirm a decrease of electric conductivity due to 1T-2H transition upon heating.

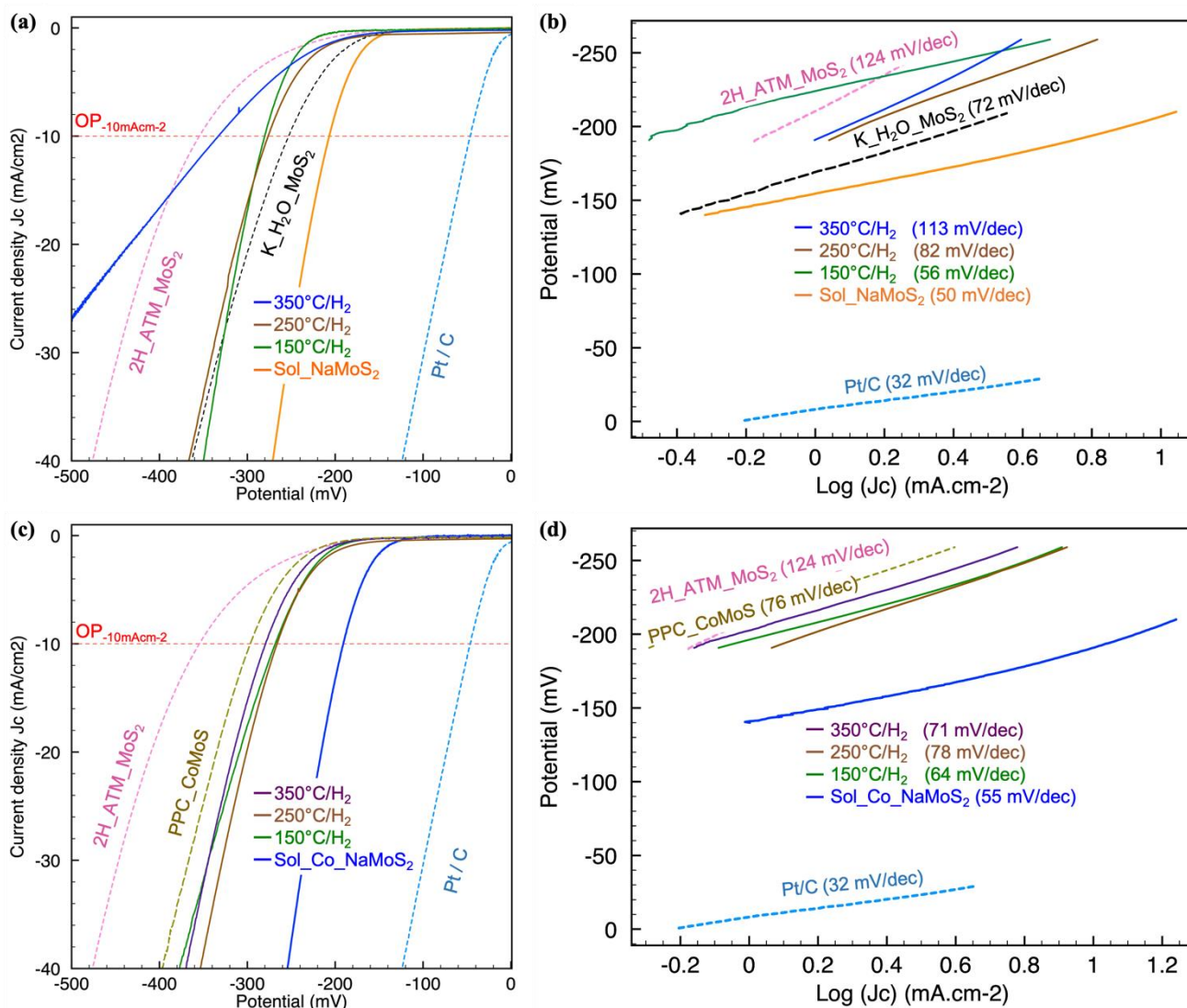


Figure 7. LSV curves obtained in 0.5 M H_2SO_4 at 5 mV/s rate (a, c) and Tafel plots (b, d) evolution as a function of pre-heating of Sol_NaMoS_2 (a,b) and Sol_Co_NaMoS_2 (c,d) materials in H_2 flow.

3.3. Catalytic properties

While 1T phase is widely investigated for electrocatalysis or batteries [47, 48], the examples of its use in thermal heterogeneous catalysis are very sparse. Potassium-promoted sulfide Mo catalysts potentially containing 1T-MoS₂ showed high activity and selectivity in methylmercaptan from syngas [49] or COS hydrogenation [50]. In combination with known high HER activity (i.e. high ability of hydrogen activation), these findings allow hypothesizing that 1-T MoS₂ could possess particular hydrogenating properties. However, in the reaction of mercaptan synthesis acid-base properties play crucial role and it seems difficult to unravel between the contribution of basic sites created by K doping and possible impact of the metallic properties and/or activity of basal planes of the 1T-phase per se.

In this work we tried to apply the lowest possible temperatures for the catalytic tests involving hydrogenation and hydrogenolysis, in order to preserve 1T phase during the catalytic reaction. With this respect, for thiophene hydrodesulfurization (HDS) reaction the situation seems borderline. The range of temperatures routinely applied in the (gas-phase) thiophene HDS lies approximately between 280 and 340 °C, which outside the domain of stability 1T phase. Indeed, deintercalation occurs near 200°C and Raman lines of 2H phase appear near the same temperature, whereas HER properties suggest that some metallic character persists up to 250°C. Therefore, HDS activity was measured from 240 °C to identify the possible contribution of 1T phase. This temperature is the lowest at which thiophene conversion is still detectable on the benchmark references on our catalytic setup. As with 1-pentene hydrogenation (HYD), the temperature might be lower than for the thiophene HDS. Conversion of 1-pentene could be observed in the presence of sulfides from 160°C onward, i.e. within the 1T-MoS₂ stability region.

Particular attention was paid to the benchmark references. The samples of bulk 2H-MoS₂ and CoMoS materials were used as external references. On the other hand, the solvothermal solids taken after *ex-situ* thermal treatment at 350°C were used as internal references. In these solids having composition similar to the initial solvothermal samples, the 1T phase was fully transformed to 2H-MoS₂. Thus, the solid Sol_Co_NaMoS₂_350°C_H₂ was considered as the 2H-polytype reference to be confronted to the initial 1T Sol_Co_NaMoS₂. Note however that the composition before and after heating was not exactly the same. Indeed, beside 1T-2H transition, EG deintercalation and other processes occur upon heating. Thus, since the parent Sol_Co_NaMoS₂ was sulfur-deficient (cf. Table S1), the XRD pattern of Sol_Co_NaMoS₂_350°C_H₂, beside the 2H-MoS₂ and Co₉S₈ phases showed MoO₂ impurity (PDF-00-032-0671). The MoO₂ phase might appear due to crystallization of the oxide species, as it happens e.g. for oxysulfide MoOS₂ [51]. Finally, *in-situ* treatment at 350°C during the catalytic test leads to irreversible 1T to 2H transformation. Therefore, comparison of the catalytic activity measured at lower temperatures (240 °C) at the beginning and at the end of the run (return points) allows accessing the role of 1T phase.

HDS activity evolves differently for the promoted and non-promoted samples (Figure 8.a-b. and Fig. S10). Bulk ATM-MoS₂ reference deactivates during the reaction, being the only catalyst for which the initial 240°C HDS activity was significantly higher than that at the return point. For this ATM-MoS₂ material, the decrease of activity is related to the collapse of micropores [52]. HDS activity of 1T-MoS₂ solvothermal solids appears considerably lower than for the ATM-MoS₂ reference. The presence of Na in these solids might be the reason of low HDS activity. However, unlike its non-promoted counterpart and despite the presence of Na, promoted solvothermal solid Sol_Co_NaMoS₂ presents HDS activity

close to that of the reference PPC_CoMoS (Fig. 8b). It could be speculated that cobalt competes with sodium for the edge sites and therefore the poisoning effect is lesser. However, the initial 1T Sol_Co_NaMoS₂ and the thermally treated Sol_Co_NaMoS₂_350°C_H₂ have very close HDS activities, which does not allow considering the role of 1T phase, but compels us to attribute it to the well-known effect of promotion with cobalt.

Raman spectra of solvothermal catalysts after HDS test displayed only the 2H polytype modes (Figure S11.a-b) confirming a complete 1T to 2H transition. This result correlates with the deteriorated HER performance of the used catalyst Sol_NaMoS₂_HDS (Table S3). By contrast for used catalyst Sol_Co_NaMoS₂_HDS, the high HER activity was preserved, probably due to the presence of Co sulfide particles. The XRD patterns for both used catalysts show a broad (002) peak with $d \approx 6.5 \text{ \AA}$, which may correspond to residual Na intercalated between the MoS₂ layers (Figure S12). TEM images of used catalysts displayed agglomerated structure (Figure S13). Chemical analysis of the samples before and after HDS test expectedly show the same Mo:Na ratio (Table S1), but the S:Mo ratio was increased after test, probably because sulfidation occurred during the HDS reaction. Both catalysts displayed an important loss in C, H and O, after HDS test, related to the EG deintercalation (Table S1).

The impact of cobalt with respect of the stabilization of 1T polymorph and catalytic properties is an important issue. Cobalt is used for decades as a promoter in HDS catalysts and different modes of its interaction with MoS₂ slabs were suggested, including intercalation. Yet, those models were dismissed and only two types of cobalt species in this type of catalysts are currently recognized: the decoration species at the edges of MoS₂ slabs (so-called “CoMoS phase”) and the nanoparticles of individual phases CoS_x. If, following a novel preparation protocol, cobalt intercalation between the MoS₂ layers and/or stabilization of 1T–MoS₂ by cobalt could be evidenced, that would have a high impact on the understanding of CoMoS systems, beyond the specific preparations described here. Unfortunately, the present study rules out intercalation of cobalt between the layers as well as its stabilizing effect on the 1T phase in the systems as prepared. The involvement of 1T phase in the HDS activity was not evidenced for promoted samples. Indeed, the initial HDS activity at 240 °C (1T phase possible) and its value at the return point (only 2H phase present) are similar (Fig 8b).

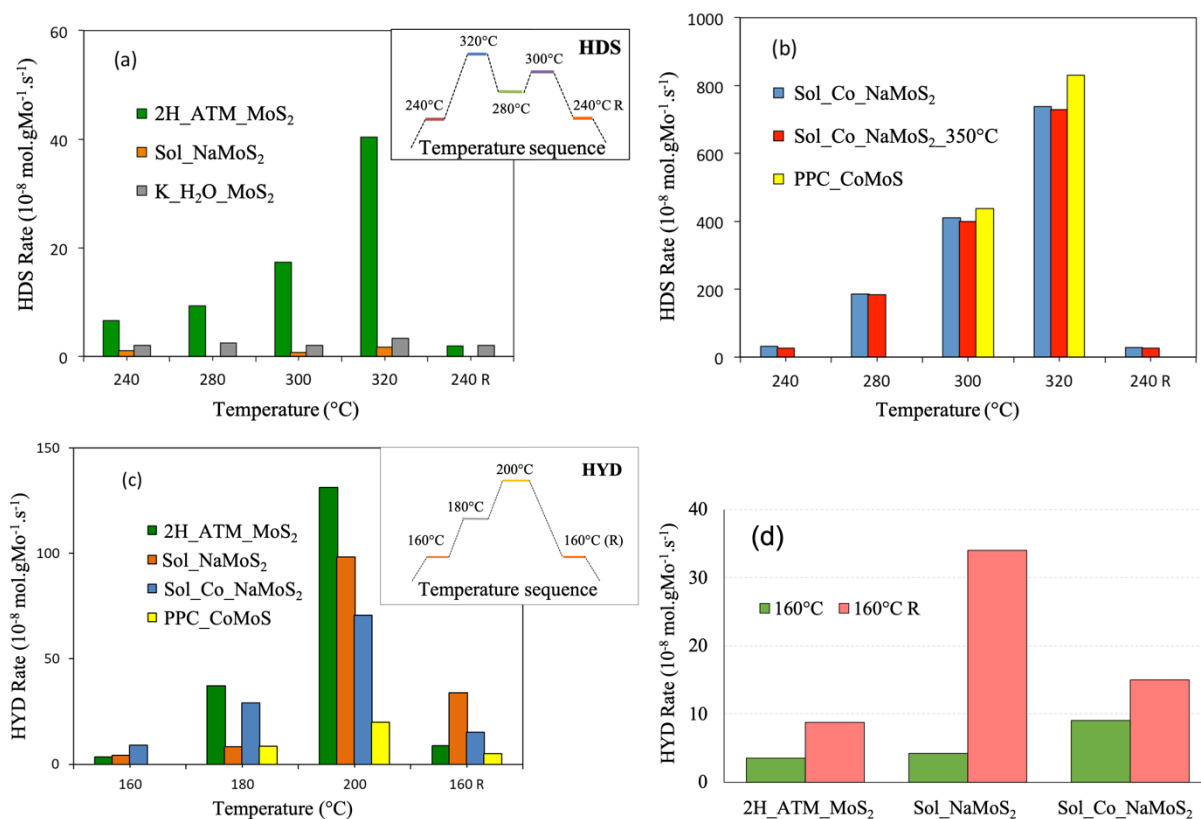


Figure 8. Specific rates of thiophene HDS, ($10^{-8} \text{ mol.gMo}^{-1}.\text{s}^{-1}$) (a,b) and 1-pentene HYD ($10^{-8} \text{ mol.gMo}^{-1}.\text{s}^{-1}$) (c, d) vs. temperature for the solvothermal catalysts under study vs. 2H-MoS₂ phase containing references. In fig (d) “R” corresponds to the return point.

We further studied the 1-pentene hydrogenation (HYD) reaction. The Sol_NaMoS₂ and Sol_Co_NaMoS₂ showed higher overall 1-pentene conversion than ATM-MoS₂ reference. Beside HYD, isomerization of 1-pentene occurred on the solvothermal samples with considerable conversions. However, isomerization is well-known to occur on the acidic sites, not involving hydrogen activation. To access the role of 1T phase we follow the same logic as for HDS tests and considered only the HYD activity. Contrary to the HDS tests, the 1T phase is stable in the HYD test at 160°C. But again, all the 1T phase was transformed to 2H phase at the end point, because higher temperatures were applied at the intermediate steps. We observed (Figure 8 d) that HYD activity at the return point (160°C) is invariably higher than the initial 160 °C activity. The solids at the initial and at the end point of HYD run have the same morphological parameters and contain the same amounts of poison species (Na ions), which makes 1T vs. 2H comparison possible. Remarkably, for Sol_NaMoS₂ catalyst there is a strong increase of HYD activity when the reaction temperature is changed from 180°C to 200°C. This strong increase matches with the 1T to 2H transition and EG deintercalation. Unlike HDS, the HYD activity does not decrease for any of the catalysts including ATM-MoS₂. Apparently, there is no sintering as the maximal temperature of HYD

catalytic tests is by 120°C lower than for HDS. The HYD activity observed at the return point is higher for the solvothermal samples than for the ATM-MoS₂ reference, suggesting the absence of poisoning effect of residual sodium for the HYD reaction. The cobalt -promoted solids are more active in HDS than the non-promoted counterparts, but present lower activity in HYD, in agreement with the absence of cobalt promotion effect on MoS₂ in the olefins HYD reaction [53].

4. Conclusion

In this work we prepared solvothermal materials containing the 1T-MoS₂ polytype then studied their stability and the catalytic properties. 1T-MoS₂ is conventionally prepared via intercalation of (*n*-BuLi) into MoS₂, followed by exfoliation. This glove-box synthesis route uses expensive reactants and presents security issues, so is quite difficult to scale-up. Solvothermal method, due to the use of inexpensive precursors, scalability and facility of operation, allows expecting large-scale preparation of 1T-MoS₂ for energy and environment applications such as catalysts, supercapacitors, water electrolysis cathodes. By this reason solvothermal and hydrothermal preparations of 1T-MoS₂ attract much attention, as potentially applicable in industry. However, understanding of the reasons and the limits of 1T-MoS₂ stabilization in such preparations are still far from being fully achieved.

Pure 1T-MoS₂, i.e. Mo(IV) sulfide with O_h coordination of molybdenum is inherently unstable. In order to stabilize 1T phase, molybdenum should be at least partially reduced to Mo(III), so the sulfide slabs should bear negative charge. Therefore, some cationic species should be present to preserve electroneutrality (protonated organic molecules, ammonium ions, alkali cations...).

Whether the resulting catalytic activity will be advantageous or not, depends not only on the presence of 1T phase under the reaction conditions, but also on the nature of stabilizing species. Thus, alkali metal cations, while ensuring good thermal stability of 1T phase, are poisonous for HDS reaction but not for the HER one.

A great number of works is published yearly on the 1T-MoS₂, which often present diverging results and controversial conclusions. Beside its primary goal of testing 1T-MoS₂ in heterogeneous catalysis, the present study contributes to sort out misconceptions and errors, overly present in the current literature. Thus, we should stress that Raman identification of 1T-MoS₂ must be carried out under inert atmosphere and should mandatory include high wavenumbers region, in order to avoid confusion with molybdenum oxide. In the same lines, we found that cobalt does not help to stabilize 1T-MoS₂. The advantageous activity observed for cobalt-containing materials, albeit in electrocatalysis or heterogeneous catalysis

reactions, comes from the formation of CoMoS phase. Tidying up this research area will hopefully help to ensure its timely progress.

References

- [1] I. Song, C. Park, H. C. Choi, Synthesis and properties of molybdenum disulphide: From bulk to atomic layers. *RSC Adv.* 5 (2015) 7495–7514
- [2] H. H. Huang, X. Fan, D. J. Singh, W. T. Zheng, Recent progress of TMD nanomaterials: phase transitions and applications, *Nanoscale* 12 (2020) 1247-1268.
- [3] W. Choi, N. Choudhary, G.H. Han, J. Park, D. Akinwande, Y.H. Lee, Recent development of two-dimensional transition metal dichalcogenides and their applications, *Mater. Today* 20 (2017) 116-130.
- [4] G. Vaitkunaite, C. Espejo, C. Wang, B. Thiébaud, C. Charrin, A. Neville, A. Morina, MoS₂ tribofilm distribution from low viscosity lubricants and its effect on friction, *Tribol. Int.* 151 (2020) 106531.
- [5] H. Toulouhat, P. Raybaud, Catalysis by transition metal sulphides from molecular theory to industrial application. *TECHNIP.* (2013).
- [6] S. Brunet, D. Mey, G. Pérot, C. Bouchy, F. Diehl, On the hydrodesulfurization of FCC gasoline: a review, *Appl. Catal. A: General* 278 (2005) 143-172.
- [7] R. Prins, M. Egorova, A. Röthlisberger, Y. Zhao, N. Sivasankar, P. Kukula, Mechanisms of hydrodesulfurization and hydrodenitrogenation, *Catal. Today* 111 (2006) 84-93.
- [8] A. Cheng, H. Zhang, W. Zhong, Z. Li, D. Cheng, Y. Lin, Y. Tang, H. Shao, Z. Li, Few-layer MoS₂ embedded in N-doped carbon fibers with interconnected macropores for ultrafast sodium storage, *Carbon.* 168 (2020) 691–700.
- [9] Y. Ma, Y. Jia, Y. Lin, W. Shi, ZnS/MoS₂ film grown on Mo foil as binder free electrode for supercapacitor, *Chem. Phys.* 542 (2021) 111030.
- [10] L. Ye, C. Wu, W. Guo, Y. Xie, MoS₂ hierarchical hollow cubic cages assembled by bilayers: one-step synthesis and their electrochemical hydrogen storage properties, *Chem. Commun.* (2006) 4738-4740.
- [11] L. Wang, L. Xie, W. Zhao, S. Liu, Q. Zhao, Oxygen-facilitated dynamic active-site generation on strained MoS₂ during photo-catalytic hydrogen evolution, *Chem. Eng. J.* 405 (2021) 127028.
- [12] P. Afanasiev, MoS₂ “inorganic fullerenes” combined with TiO₂ in water-methanol suspensions: Highly active hydrogen production photo catalysts operating via transfer of accumulated electrons, *Int. J. Hydr. Energy.* 45 (2020) 14696–14712.
- [13] A. B. Laursen, S. Kegnaes, S. Dahl, I. Chorkendorff, Molybdenum sulfides—efficient and viable materials for electro - and photoelectrocatalytic hydrogen evolution, *Energy Environ. Sci.* 5 (2012) 5577-5591.
- [14] L. Wang, X. Liu, Q. Zhang, G. Zhou, Y. Pei, S. Chen, J. Wang, A.M. Rao, H. Yang, B. Lu, Quasi-one-dimensional Mo chains for efficient hydrogen evolution reaction, *Nano Energy.* 61 (2019) 194–200.
- [15] E. Ramírez-Mondragón, O. E. Contreras, U. J. Tamayo-Pérez, M. T. Oropeza-Guzmán, Synthesis and characterization of Ni₂P and MoS₂ on MWCNT as an innovative catalytic material for hydrogen generation, *Appl. Surf. Sci.* 503 (2020) 144163.
- [16] M. A. Py, R. R. Haering, Structural destabilization induced by lithium intercalation in MoS₂ and related compounds. *Can. J. Phys.* 61(1983) 76-84.
- [17] F. Wypych, R. Schollhorn, 1T-MoS₂, a new metallic modification of molybdenum disulfide. *J. Chem. Soc. Chem. Commun.* 19 (1992) 1386-1388.
- [18] J. Bai, B. C. Zhao, J. F. Zhou, J. G. Si, Z. T. Fang, K. Z. Li, H. Y. Ma, J. M. Dai, X. B. Zhu, Y. P. Sun, Glucose-induced synthesis of 1T-MoS₂/C hybrid for high-rate lithium-ion batteries, *Small* 15 (2019) 1805420.
- [19] M. Acerce, D. Voiry, M. Chhowalla, Metallic 1T phase MoS₂ nanosheets as supercapacitor electrode

materials. *Nat. Nanotech.* 10 (2015) 313–318.

[20] L. Wang, X. Liu, J. Luo, X. Duan, J. Crittenden, C. Liu, S. Zhang, Y. Pei, Y. Zeng, X. Duan, Self-Optimization of the Active Site of Molybdenum Disulfide by an Irreversible Phase Transition during Photocatalytic Hydrogen Evolution, *Angew. Chem. Int. Ed.* 56 (2017) 7610–7614.

[21] H. Topsøe, The Role of Co–Mo–S Type Structures in Hydrotreating Catalysts, *Appl. Catal. A* 322 (2007) 3–8.

[22] J. Kibsgaard, Z. Chen, B. N. Reinecke, T. F. Jaramillo, Engineering the surface structure of MoS₂ to preferentially expose active edge sites for electrocatalysis *Nature Mater.* 11 (2012) 963–969.

[23] D. Voiry, M. Salehi, R. Silva, T. Fujita, M. Chen, T. Asefa, V. B. Shenoy, G. Eda, M. Chhowalla, Conducting MoS₂ Nanosheets as Catalysts for Hydrogen Evolution Reaction. *Nano Lett.* 13 (2013) 6222–6227.

[24] X-L Fan, Y. Yang, P. Xiao, W.-M. Lau, Site-specific catalytic activity in exfoliated MoS₂ single-layer polytypes for hydrogen evolution: basal plane and edges, *J. Mater Chem. A*, 48 (2014) 20545–2551.

[25] M. Yu, N. Kosinov, L. van Haandel, P. J. Kooyman, E. J. M. Hensen, Investigation of the Active Phase in K-Promoted MoS₂ Catalysts for Methanethiol Synthesis, *ACS Catal.* 10 (2020) 1838–1846.

[26] A. Cordova, P. Blanchard, C. Lancelot, G. Frémy, C. Lamonier, Probing the Nature of the Active Phase of Molybdenum-Supported Catalysts for the Direct Synthesis of Methylmercaptan from Syngas and H₂S, *ACS Catal.* 5 (2015) 2966–2981.

[27] X. Wang, X. Shen, Z. Wang, R. Yu, L. Chen, Atomic-Scale Clarification of Structural Transition of MoS₂ upon Sodium Intercalation, *ACS Nano* 8 (2014) 11394–11400.

[28] K. Ai, C. Ruan, M. Shen, L. Lu, MoS₂ nanosheets with widened interlayer spacing for high-efficiency removal of mercury in aquatic systems, *Adv. Funct. Mater.*, 26 (2016) 5542–5549.

[29] Z. Li, R. Fan, Z. Hu, W. Li, H. Zhou, S. Kang, Y. Zhang, H. Zhang, G. Wang, Ethanol introduced synthesis of ultrastable 1T-MoS₂ for removal of Cr(VI), *Journal of Hazardous Materials*, 394 (2020) 122525

[30] X. Li, T. Qian, J. Zai, K. He, Z. Feng, X. Qian, Co stabilized metallic 1Td MoS₂ monolayers: Bottom-up synthesis and enhanced capacitance with ultra-long cycling stability, *Mater. Today En.* 7 (2018) 10–17.

[31] A. Taufik, Y. Asakura, H. Kato, M. Kakihana, R. Saleh, Tohru Sekino, S. Yin, 1T/2H-MoS₂ engineered by in-situ ethylene glycol intercalation for improved toluene sensing response at room temperature, *Adv. Powder Tech.*, 31, 5 (2020), 1868–1878.

[32] A. Hadj-Aïssa, F. Dassenoy, C. Geantet, P. Afanasiev, Solution synthesis of core–shell Co₉S₈@MoS₂ catalysts, *Catal. Sci. Technol.* 6 (2016) 4901–4909.

[33] E. Blanco, D. Uzio, G. Berhault, P. Afanasiev, From core–shell MoS_x/ZnS to open fullerene-like MoS₂ nanoparticles, *J. Mater. Chem. A*. 2 (2014) 3325–3331.

[34] S. Palencia-Ruiz, D. Laurenti, D. Uzio, C. Legens, P. Afanasiev, Facile ambient pressure propylene carbonate solution synthesis of highly divided CoMoS solids, *Mater. Let.* (2020) 128296.

[35] J. Zheng, H. Zhang, S. Dong, Y. Liu, C. T. Nai, H. S. Shin, H. Y. Jeong, B. Liu, K. P. Loh . High yield exfoliation of two-dimensional chalcogenides using sodium naphthalenide. *Nat. Commun.* 5 (2014) 1–7.

[36] R. Bissessur., D. Gallant, R. Brüning, Novel nanocomposite material consisting of poly [oxymethylene-(oxyethylene)] and molybdenum disulfide. *Mater. Chem. Phys.* 82 (2003) 316–320.

[37] R. Bissessur, J. L. Schindler, C. R. Kannewurf, Encapsulation of Polymers into MoS₂ and Metal to Insulator Transition in Metastable, *J. Chem. Soc.* 245 (1994) 249–254.

[38] M. G. Kanatzidis, R. Bissessur, D. C. DeGroot, J. L. Schindler, C. R. Kannewurf. New Intercalation Compounds of Conjugated Polymers. Encapsulation of Polyaniline in MoS₂. *Chem. Mater.* 5 (1993) 595–596.

[39] X. Gan, L. Y. S. Lee, K. Wong, T. W. Lo, K. H. Ho, D. Y. Lei, H. Zhao, 2H/1T Phase Transition of Multilayer MoS₂ by Electrochemical Incorporation of S Vacancies. *ACS Appl. Energy Mater.* 1. 4754–4765 (2018).

[40] L. Cai, J. He, Q. Liu, T. Yao, L. Chen, W. Yan, F. Hu, Y. Jiang, Y. Zhao, T. Hu, Z. Sun, S. Wei, Vacancy-Induced Ferromagnetism of MoS₂ Nanosheets. *J. Am. Chem. Soc.* 137 (2015). 2622–2627.

-
- [41] Q. Li, Z. Yao, J. Wu, S. Mitra, S. Hao, T. Subra Sahu, Y. Li, C. Wolverton, V. Dravid, Intermediate phases in sodium intercalation into MoS₂ nanosheets and their implications for sodium-ion batteries. *Nano Energy* 38, (2017), 342-349.
- [42] Papageorgopoulos. C. A. & Jaegermann. W. Li intercalation across and along the van der Waals surfaces of MoS₂(0001). *Surf. Sci.* 338 (1995) 83-93.
- [43] J.R.S. Tan, I. Abdelwahab, Z. Ding, X. Zhao, T. Yang, G. Z. J. Loke, H. Lin, I. Verzhbitskiy, S. M. Poh, H. Xu, C. T. Nai, W. Zhou, G. Eda, B. Jia, K. P. Loh,. Chemical Stabilization of 1T' Phase Transition Metal Dichalcogenides with Giant Optical Kerr Nonlinearity. *J. Am. Chem. Soc.* 139 (2017) 2504–2511.
- [44] Y. Xiao, M. Tan, Z. Li, L. He, B. Gao, Y. Chen, Y. Zheng, B. Lin, Ethylenediamine-assisted phase engineering of 1T/2H–MoS₂/graphene for efficient and stable electrocatalytic hydrogen evolution, *Int. J. Hydr. Energy.* 46 (2021) 11688–11700.
- [45] S. Duraisamy, A. Ganguly, P.K. Sharma, J. Benson, J. Davis, P. Papakonstantinou, One-Step Hydrothermal Synthesis of Phase-Engineered MoS₂/MoO₃ Electrocatalysts for Hydrogen Evolution Reaction, *ACS Appl. Nano Mater.* 4 (2021) 2642–2656.
- [46] S. Pang, B.-H. Wee, S. Chin, The Capacitive Behaviors of Manganese Dioxide Thin-Film Electrochemical Capacitor Prototypes, *International J. Electrochem.* (2011) 397685.
- [47] A. Saha, A. Paul, D.N. Srivastava, A.B. Panda, Exfoliated colloidal MoS₂ nanosheet with predominantly 1T phase for electrocatalytic hydrogen production, *Int. J. Hydr. Energy.* 45 (2020) 18645–18656.
- [48] S.-H. Moon, M.-C. Kim, J.-H. Choi, Y.-S. Kim, H. Kim, K.-W. Park, 1T-MoS₂/carbon nanofiber composite as an interlayer fabricated by an in situ electrochemical fabrication method for lithium-sulfur batteries, *J. Alloys Compounds.* 857 (2021) 158236.
- [49] A. Cordova, P. Blanchard, C. Lancelot, G. Frémy, C. Lamonier, Probing the Nature of the Active Phase of Molybdenum-Supported Catalysts for the Direct Synthesis of Methylmercaptan from Syngas and H₂S, *ACS Catal.* 5 (2015) 2966–2981.
- [50] O. Y. Gutiérrez, C. Kaufmann, A. Hrabar, Y. Zhu, J. A. Lercher, Synthesis of methyl mercaptan from carbonyl sulfide over sulfide K₂MoO₄/SiO₂, *J. Catal.* 280 (2011) 264–273.
- [51] D. Genuit, I. Bezverkhyy, P. Afanasiev, Solution preparation of the amorphous molybdenum oxysulfide MoOS₂ and its use for catalysis, *J. Solid State Chem.* 178 (2005) 2759-2765.
- [52] P. Afanasiev, The influence of reducing and sulfiding conditions on the properties of unsupported MoS₂-based catalysts, *J. Catal.* 269 (2010) 269-280.
- [53] S. Brunet, D. Mey, G. Pérot, C. Bouchy, F. Diehl, On the hydrodesulfurization of FCC gasoline: a review, *Applied Catalysis A: General.* 278 (2005) 143–172.

Highlights

Stability and catalytic properties of 1T-MoS₂ obtained via solvothermal synthesis

- ▶ Nanodispersed 1T-(Co)MoS₂ prepared by solvothermal technique
- ▶ 1T-(Co)MoS₂ shows high activity in HER but not in hydrogenation and hydrodesulfurization
- ▶ Stabilization of 1T-MoS₂ occurs due to ethylene glycol intercalation
- ▶ Cobalt does not stabilize 1T phase but improves HER and HDS activity

Graphical abstract

